Title

Chapter One Saturation Recovery EPR and Nitroxide Spin Labeling for Exploring Structure and Dynamics in Proteins

Authors

Yang, Zhongyu
Bridges, Michael
Lerch, Michael T
et al.

Publication Date

2015

DOI

10.1016/bs.mie.2015.07.016

CHAPTER ONE

Saturation Recovery EPR and Nitroxide Spin Labeling for Exploring Structure and Dynamics in Proteins

Zhongyu Yang, Michael Bridges, Michael T. Lerch, Christian Altenbach, Wayne L. Hubbell[1]

Jules Stein Eye Institute and Department of Chemistry and Biochemistry, University of California, Los Angeles, California, USA

[1]Corresponding author: e-mail address: hubbellw@jsei.ucla.edu

Contents

Abstract

Experimental techniques capable of determining the structure and dynamics of proteins are continuously being developed in order to understand protein function. Among existing methods, site-directed spin labeling in combination with saturation recovery (SR) electron paramagnetic resonance spectroscopy contributes uniquely to the determination of secondary and tertiary protein structure under physiological conditions, independent of molecular weight and complexity. In addition, SR of spin labeled proteins was recently demonstrated to be sensitive to conformational exchange events with characteristic lifetimes on the order of μs, a time domain that presents a significant challenge to other spectroscopic techniques. In this chapter, we present the theoretical background necessary to understand the capabilities of SR as applied to spin labeled proteins, the instrumental requirements, and practical experimental considerations necessary to obtain interpretable data, and the use of SR to obtain information on protein: (1) secondary structure via solvent accessibility measurements, (2) tertiary structure using interspin distance measurements, and (3) conformational exchange.

Methods in Enzymology, Volume 564
ISSN 0076-6879
http://dx.doi.org/10.1016/bs.mie.2015.07.016

1. INTRODUCTION

Saturation recovery (SR) electron paramagnetic resonance (EPR) methodology was developed by Hyde in the 1970s to measure the electron spin–lattice relaxation time (T_{1e}) of paramagnetic species (Huisjen & Hyde, 1974; Percival & Hyde, 1975). It has been extensively employed with nitroxide spin labels to investigate the dynamics of lipids in membranes (Kawasaki, Yin, Subczynski, Hyde, & Kusumi, 2001; Popp & Hyde, 1982; Yin, Pasenkiewicz-Gierula, & Hyde, 1987) and to determine the diffusivity of oxygen in membranes (Kusumi, Subczynski, & Hyde, 1982; Subczynski, Hyde, & Kusumi, 1989, 1991; Yin & Hyde, 1987). This chapter focuses on recent developments that combine SR and site-directed spin labeling (SDSL) to explore structure and internal dynamics of proteins. The most commonly used nitroxide in SDSL is the side chain designated R1, introduced by cysteine substitution mutagenesis followed by reaction with a sulfhydryl-specific methanethiosulfonate reagent (Fig. 1A). Interpretation of the EPR spectra of R1 in proteins is greatly aided by the extensive information that is available on structure and dynamics for this side chain (Columbus & Hubbell, 2004; Columbus, Kálai, Jekö, Hideg, & Hubbell, 2001; Fleissner, Cascio & Hubbell, 2009). Applications of SR presented below will be restricted to proteins containing this side chain and derivatives thereof, although the principles are the same for other nitroxide side chains.

For an ensemble of paramagnets at equilibrium in an external magnetic field, there is a macroscopic magnetization vector with a longitudinal component M_z along the field direction, and transverse components M_x and M_y orthogonal to M_z. If the Boltzmann distribution of the spin population is perturbed in some way, thermodynamic equilibrium of M_z is restored through interactions with the surroundings (the "lattice") by the process of spin–lattice relaxation. In the case of an ensemble of noninteracting spins in dilute solution, its recovery to an equilibrium state is exponential according to,

$$M_z(t) = M_z(\text{eqm}) + [M_z(0) - M_z(\text{eqm})]\exp(-t/T_{1e}) \quad (1)$$

where $M_z(t)$, M_z(eqm), and $M_z(0)$ are the magnetization values at any time t, at equilibrium, and immediately after the perturbation, respectively, and T_{1e} is the spin–lattice relaxation time. The amplitude of a continuous wave (CW) EPR spectrum is proportional to M_z, and the recovery to equilibrium can be followed by recording the amplitude as a function of time. For R1 in

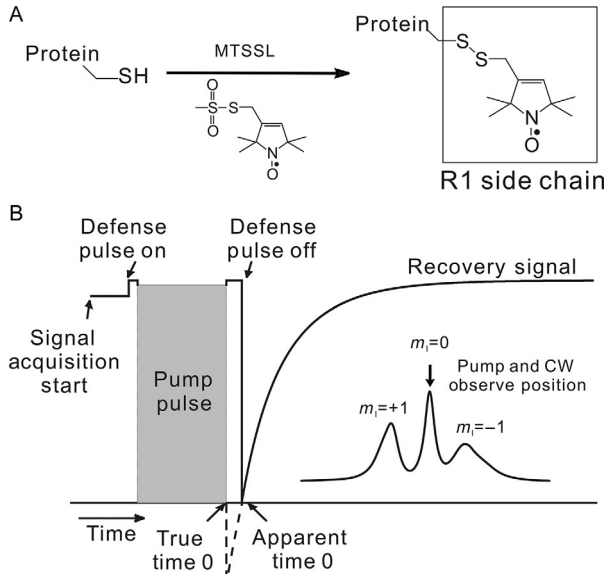

Figure 1 Site-directed spin labeling and saturation recovery EPR. (A) The introduction of the R1 side chain via the reaction of a nitroxide methanethiosulfonate reagent with cysteine (Berliner, Grunwald, Hankovszky, & Hideg, 1982). (B) The time course of a long-pulse saturation recovery experiment. An excitation (pump) pulse located at the field position of maximum intensity in the EPR absorption spectrum (see inset) causes saturation of the electron spin system. Low-power CW detection (CW observe) at the same field position records the signal recovery. The "defense pulse" is required to protect the detector electronics, and the earliest time points of the recovery signal beginning at the true time 0 are not recorded.

proteins, T_{1e} is on the order of microseconds at room temperature at X-band (~9.5 GHz) EPR frequencies. The microwave frequency dependence and mechanisms that give rise to nitroxide spin–lattice relaxation in fluid solution have been investigated (Froncisz et al., 2008; Mailer, Nielsen, & Robinson, 2005; Owenius, Terry, Williams, Eaton, & Eaton, 2004; Robinson, Haas, & Mailer, 1994; Sato et al., 2008), and interested readers should consult relevant references for details.

For topics discussed in this chapter, the most useful features that influence the apparent T_{1e} for a nitroxide attached to a protein are (1) the rotational correlation time (τ_R) of the nitroxide, in the range of 1–10 ns (Bridges, Hideg, & Hubbell, 2010; Sato et al., 2008); (2) the Heisenberg exchange frequency with another freely diffusing paramagnetic species "R_{ex}" (Altenbach, Froncisz, Hemker, McHaourab, & Hubbell, 2005; Pyka, Ilnicki, Altenbach, Hubbell, & Froncisz, 2005); (3) the distance-dependent

enhancement of nitroxide T_{1e} due to the presence of a paramagnetic metal ion with relatively long T_{1e} (Eaton & Eaton, 2002); and (4) exchange between different environments that takes place on the time scale of T_{1e} (Bridges et al., 2010; Kawasaki et al., 2001). Both (1) and (2) depend on the local structure of the protein around R1, while (3) can provide information on global structure in a protein via distance measurements between a bound metal ion and nitroxide. Exchange effects (4) can arise in cases where two conformations of a spin labeled protein coexist at equilibrium. In such cases, the presence of exchange events can be identified from measurement of effective T_{1e} values. Thus, measurement of T_{1e} under the appropriate conditions can provide information on both static and dynamic features of a protein and applications that make use of the above dependencies will be outlined below.

2. THEORETICAL BACKGROUND AND THE MEASUREMENT OF T_{1e} WITH SR

The methodology and theory of SR has been considered in detail in the literature (Eaton & Eaton, 2005; Freed, 1974; Percival & Hyde, 1975; Robinson et al., 1994), and here, we outline the main results relevant to R1 in proteins and the applications mentioned above. Figure 1B illustrates a typical SR experiment for the commonly employed ^{14}N nitroxide, where an intense pulse of microwave radiation (the "pump") is applied to the absorption maximum of the central ($m_I = 0$) resonance line. If the pump has sufficient microwave power, the spin system will be saturated in the sense that $M_z(0)$, and thus the CW-detected EPR signal amplitude is zero. The receiver of the spectrometer is protected from effects of the intense pump pulse with a defense pulse that transiently blocks the signal path; the length of the defense pulse sets the dead time of the experiment. Low-intensity CW microwave radiation (the "observe") monitors the return of the EPR signal to equilibrium, which is proportional to $M_z(t)$.

In general, the recovery of $M_z(t)$ for a single population of nitroxides, including the effects of Heisenberg exchange, is a sum of exponentials (Haas, Mailer, Sugano, & Robinson, 1992; Pyka et al., 2005) with the following time dependence:

$$f(t) = A_1 e^{-(2W_e + 2W_{ex})t} + A_2 e^{-(2W_e + 2W_{ex} + 3W_n)t} + A_3 e^{-(2W_e + 2W_{ex} + 2W_R)t} + A_4 e^{-(2W_e + 2W_{ex} + 3W_n + 2W_R)t} + \text{H.O.T} \quad (2)$$

where the W values are relaxation rates of various processes that contribute to recovery from saturation: $W_e = (2T_{1e})^{-1}$ is the direct electron spin–lattice relaxation rate, W_{ex} is the Heisenberg exchange rate in the presence of R_{ex}, W_n is the rate of nitrogen nuclear relaxation, a process that couples the nitroxide hyperfine components $m_I = 1, 0, -1$ (Fig. 1B), and $W_R = \tau_R^{-1}$ is the rotational rate of the nitroxide; H.O.T are higher order terms considered to be insignificant (Pyka et al., 2005; Sugano, Mailer, & Robinson, 1987). Rotational motion of the nitroxide and nuclear relaxation lead to transfer of saturation to different regions of the spectrum, a process generally referred to as spectral diffusion (Fleissner et al., 2011; Haas, Sugano, Mailer, & Robinson, 1993).

For the majority of studies where T_{1e} is of interest, the correlation time of the nitroxide for R1 in a protein is in the range of 1–10 ns (the intermediate motional regime). For example, the shortest correlation time for R1 in a folded protein is dictated by the internal motion of R1 at surface sites, for which $\tau_R \approx 1.5$–2.5 ns (Columbus et al., 2001). For R1 at a buried site, or for a rigidly attached nitroxide side chain (Fleissner et al., 2011; Guo, Cascio, Hideg, Kálái, & Hubbell, 2007), τ_R is determined by the rotational diffusion of the entire protein, which for a small globular proteins of M.W. $\approx$ 20 kDa is approximately 6 ns in aqueous solution at room temperature. In this intermediate motional regime, W_R and W_n are on the order of 100 and 10 MHz, respectively (Robinson et al., 1994), while W_e is on the order of 0.1 MHz. Thus, the spectral diffusion processes are 2–3 orders of magnitude faster than W_e; if the duration of the saturating pump pulse is $\geq\sim$500 ns, these processes are complete within the pump time and do not contribute significantly to the recovery curve. For this "long-pulse" SR experiment, with pump durations typically in the 1–4 μs range (Hyde, 1979), only the first term in Eq. (2) is important and a true spin–lattice relaxation time can be observed in the absence of Heisenberg exchange. For very fast ($\tau_R < 1$ ns) or very slow ($\tau_R > 10$ ns) nitroxide motions, spectral diffusion due to W_n will contribute to the recovery and must be considered; W_R contributes to the recovery if $\tau_R \gg 10$ ns (Fleissner et al., 2011; Haas et al., 1992). The spectral diffusion terms are themselves of interest to measure slow protein dynamics and can be extracted with SR measurements in tandem with the electron–electron double resonance (ELDOR) technique, a method closely related to SR but where pump and observe frequencies are different; a discussion of this method is beyond the scope of this chapter, and the interested reader is referred to the literature (Fleissner et al., 2011; Haas et al., 1993; Hyde, Chien, & Freed, 1968).

For a single-spin population, and in the absence of spectral diffusion and Heisenberg exchange, Eq. (2) predicts a single-exponential recovery of $M_z(t)$ following a saturating pulse. However, conventional EPR spectrometers do not measure $M_z(t)$ directly, but rather the CW observe beam monitors the transverse magnetization $M_y(t)$ that is proportional to $M_z(t)$, and the experimentally detected recovery signal, $S(t)$, includes additional time-dependent terms according to (Percival & Hyde, 1975):

$$S(t) \propto M_{y0} \exp\left(-\frac{t}{T_{2e}}\right) + \gamma_e B_1 T_{2e}\left[\frac{M_{z0} - M_{z\infty}}{1+\gamma_e^2 B_1^2 T_{1e} T_{2e}}\right] \exp\left(-\frac{t}{T_{1e}} - \gamma_e^2 B_1^2 T_{2e} t\right) + \frac{M_{z\infty}\gamma_e B_1 T_{2e}}{1+\gamma_e^2 B_1^2 T_{1e} T_{2e}} - M_{z0}\gamma_e B_1 T_{2e} \exp\left(-\frac{t}{T_{2e}}\right) \quad (3)$$

where M_{y0} and M_{z0} are the magnetizations along on the y- and z-axes, respectively, at time zero after a pump pulse, $M_{z\infty}$ is the equilibrium magnetization along z, T_{2e} is the electron spin transverse relaxation time, γ_e the electron gyromagnetic ratio, and B_1 the magnetic field strength of the observe beam. The term highlighted in gray is the desired SR, and the third term is simply the steady-state CW EPR spectral amplitude, a term that does not affect the time course of the recovery. The first term, the "free induction decay" (FID), and the fourth term are undesirable and, in principle, may complicate analyses of the recovery curves. In practice, these terms that involve "$\exp(-t/T_{2e})$" cause little complication for experiments with nitroxides in the correlation time range of 1–10 ns where $T_{2e} \ll T_{1e}$, and these terms may vanish within the effective dead time of the instrumentation defined by the defense pulse. Under any circumstance, however, the FID term is removed by a phase cycling procedure implemented in the commercially available instruments from Bruker Biospin. Alternatively, a microwave source that is not coherent with the observe source can be used as a pump to eliminate the FID; the ELDOR arm in a Bruker Elexsys 580 (E580) so equipped is such a source. The fourth term can be eliminated by a sufficiently high pump power to achieve complete saturation, i.e., where $M_{z0} = 0$. It is prudent to confirm the absence of these terms in the recovery as described by Hyde (1979).

Of particular importance is the presence of the quantity $-\gamma_e^2 B_1^2 T_{2e}^t$ that adds to $-t/T_{1e}$ in the exponential of the SR signal and shortens the apparent recovery time constant. The magnetic field of the observe beam is related to the microwave power according to $B_1 = \sqrt{QP_1}$ where Q is the quality

factor of the resonator and P_1 is the incident observe microwave power. B_1 multiplies all terms in Eq. (3) except the FID, and the observe microwave power should be as large as possible to insure acceptable signal to noise in the detected signal, but must sufficiently low not to substantially shorten the recovery time.

In summary, the pure SR signal is observed with phase cycling to remove the FID, with low observe power, and sufficiently high pump power so that $M_{z0} \approx 0$. Practical considerations for achieving these conditions are discussed in the next section.

3. INSTRUMENTATION AND PRACTICAL CONSIDERATIONS

Commercial instrumentation for SR is available as part of the E580 spectrometer from Bruker Biospin. In the SR spectrometer, unlike the conventional CW EPR spectrometer, magnetic field modulation is not employed in the detection of the CW observe signal, and a large number of transient SR curves are averaged, typically 1–2 million. The repetition rate is determined by the T_{1e} of the sample, and the time between pump pulses is conservatively selected to be $\approx 5 \times T_{1e}$. Field-independent instrumental artifacts due to switching transients and resonator heating from the pump pulse are canceled by subtracting signals recorded on- and off-resonance; the off-resonance signal is obtained by stepping the magnetic field at a rate suitable for field stabilization ($\approx$1 Hz for the Bruker E580). The entire process of data acquisition, including phase cycling to remove the FID and field-stepping for baseline correction, is fully automated under software control.

The resonator used in this laboratory with the Bruker E580 is a 2-loop-1-gap resonator (LGR) with a sample loop of 1 mm diameter $\times$ 5 mm length (Hubbell, Froncisz, & Hyde, 1987). LGRs are well suited for SR measurement due to a short ring-down time for the pump pulse resulting from their relatively low Q (<1000), a high sample filling factor that gives good detection sensitivity, and a high efficiency for conversion of incident power to microwave magnetic field in the resonator (Hyde, Yin, Froncisz, & Feix, 1985). The short ring-down time $t_{RD} = Q/2\pi\nu \approx 20$ ns, where ν is the spectrometer frequency, means that data collection can occur $\approx$100 ns after the pump pulse termination, allowing for measurement of relatively short $T_{1e}s$ ($\approx$0.5 μs). The high conversion efficiency means that relatively low-incident microwave powers are needed for complete saturation

of the spin system. The Bruker split-ring resonator ER 4118X-MS2 has similar properties and is also well suited for SR.

The presence of paramagnetic oxygen in liquid samples shortens the apparent T_{1e} of a nitroxide by Heisenberg exchange. Dissolved oxygen in the sample is conveniently removed by flowing nitrogen gas over the sample contained in a gas-permeable sample tube made of TPX plastic or thin-walled Teflon. TPX capillaries of 0.6 mm (I.D.) × 0.8 mm (O.D.) are commercially available (Molecular Specialties, Inc. and Bruker Biospin) and are compatible with both the LGR and Bruker split-ring resonator; the active volume of the sample is ≈2.5 μL, and spin concentrations are typically in the range of 100–500 μ*M*. Nitrogen flow is conveniently provided by the Bruker temperature control unit (ER 4131VT) which employs nitrogen gas as the heat transfer medium.

As is evident from the previous section and Eq. (3), proper selection of the pump pulse duration and power and the CW observe power is essential for interpretation of SR data. Detailed considerations for selecting these parameters have been published (Eaton & Eaton, 2005; Hyde, 1979), and the key points are summarized here. For all applications considered in this chapter, suppression of spectral diffusion is desired and long-pulse SR is employed. Typically, a 1–4 μs pump is sufficient for R1 in a protein where τ_R is in the 1–10 ns, but this should be confirmed by investigating the time course of recovery as a function of pump pulse length; the pump length is increased until the observed time constant(s) become independent of pulse length. The pump power should be sufficiently high to achieve saturation, thereby suppressing the fourth term in Eq. (3) by making $M_{z0} \approx 0$. Experimentally, the pump power is increased until the amplitude and time constant of the recovery signal become essentially independent of pump power. The amplitude of the recovery will increase with increasing pump power because the recovery amplitude is proportional to $|M_{z0} - M_{z\infty}|$ and is largest when $M_{z0} = 0$ at high power and complete saturation (2nd term, Eq. 3). Using the highest power available and very long pulses would appear to be best, but resonator heating becomes a problem at high powers and long durations, so optimization is necessary. Incident pump powers on the order of 200 mW are typical for the LGR.

As the power of the CW observe beam is increased, the amplitude of the recovery increases; note that the third term in Eq. (3) is the amplitude of the CW signal at $t = \infty$, and this is proportional to B_1, which is in turn proportional to the square root of observe power. On the other hand, B_1 shortens the apparent T_{1e} by the quantity $\gamma_e^2 B_1^2 T_{2e}$, so the observe power must also be

optimized for maximum signal with an acceptable perturbation of T_{1e}. Again, the optimum observe power will depend on the resonator and is on the order of 100 μW for the LGR. Despite the effect on T_{1e}, high observing powers can be used in the SR determination of Heisenberg exchange rates with negligible error (Yin & Hyde, 1989); the enhancement of signal strength is dramatic.

With the above considerations, a good approximation to the true T_{1e} can be obtained. For a single-spin population, single-exponential recoveries should always be obtained when the pump and observe parameters are optimized.

4. APPLICATIONS OF LONG-PULSE SR

4.1 Resolving Protein Secondary Structure via Solvent Accessibility

Sequence-correlated R1 solvent accessibility encodes a remarkable amount of information on a protein fold, including the type of regular secondary structure and its orientation within the tertiary fold (Altenbach et al., 2005; Isas, Langen, Haigler, & Hubbell, 2002). For membrane-bound proteins, the topology of the structure with respect to the membrane surface can be determined (Hubbell & Altenbach, 1994; Hubbell, Gross, Langen, & Lietzow, 1998; Oh et al., 1996).

In SDSL, the solvent accessibility of R1 in a protein is measured via the collision rate of the nitroxide with a paramagnetic species in solution (R_{ex}) that has a T_{1e} much shorter than that for the nitroxide. The collision results in Heisenberg (electron) spin exchange, which appears as a spin–lattice relaxation event for the nitroxide, and the T_{1e} of the nitroxide is shortened in proportion to the Heisenberg exchange rate (W_{ex}),

$$W_{ex} = j_{ex} C_R = \left[\frac{1}{T_{1e}(R)} - \frac{1}{T_{1e}(0)} \right] \tag{4}$$

where $T_{1e}(R)$ and $T_{1e}(0)$ are the spin–lattice relaxation rates of the nitroxide in the presence and absence of a relaxation reagent, respectively, C_R is the concentration of R_{ex} and j_{ex} is the Heisenberg exchange rate constant. The spin–lattice relaxation rates are conveniently measured by SR with the considerations given above, and j_{ex} is determined from Eq. (4) as a direct measure of solvent accessibility. Although j_{ex} may be estimated from a single value of C_R, typically j_{ex} is determined from the slope of a plot of

W_{ex} versus C_R. A more detailed analysis of Heisenberg exchange as a measure of accessibility is provided by Altenbach et al. (2005), wherein the Heisenberg exchange rate constant was designated k_{ex}; here k_{ex} is reserved for conformational exchange and j_{ex} is used for Heisenberg exchange.

The choice of R_{ex} is determined by the information sought. The most commonly used species for mapping of solvent accessibility are the paramagnetic metal complex Nickel (II) EDDA (NiEDDA) and molecular oxygen, both of which have T_{1e} values that are significantly shorter than those of nitroxides (Bertini, Luchinat, & Parigi, 2001; Teng, Hong, Kiihne, & Bryant, 2001). In addition, both reagents are electrically neutral, thus ensuring that W_{ex} is not influenced by the local electrostatic potential of the protein. The two reagents differ in size and polarity, and the larger NiEDDA gives a higher contrast between exposed and partially buried sites, whereas O_2 provides improved contrast among partially buried sites (Isas et al., 2002). Typical concentrations of R_{ex} used to induce detectable changes in apparent T_{1e} relaxation are low, on the order of 0–1.5 mM for NiEDDA and 0–0.26 mM for oxygen. Under these conditions, these R_{ex} generally do not perturb the protein structure.

Heisenberg exchange with charged R_{ex} has been used to measure local electrostatic potential using CW methods (Lin et al., 1998; Shin & Hubbell, 1992), and extensions using SR are straightforward. Indeed, the many applications that have employed CW saturation methods for estimating Heisenberg exchange can in future studies enjoy the benefits of direct measure by SR. One of the most important advantages of SR compared to CW saturation is the ability to detect multiple populations of nitroxides with different $T_{1e}s$. For example, if a protein exists in two conformations where R1 has a different T_{1e} in each, in general the SR relaxation will be biexponential and the individual accessibilities can be determined (Pyka et al., 2005).

An example of using SR to measure solvent accessibility is shown in Fig. 2, where R1 was introduced sequentially (a "nitroxide scan") at sites 128 through 135 in an α-helix of T4 lysozyme (Fig. 2A). The oxygen- and NiEDDA-dependent j_{ex} values and the intrinsic spin–lattice relaxation rates for each site were determined using methods described above. A clear periodicity can be observed for both reagents, reflecting the helical structure of the protein (Fig. 2B). In this case, W_e values determined in the absence of R_{ex} show a similar periodicity (Fig. 2B) due to the approximately linear dependence of W_e on the nitroxide correlation time (Fig. 2C) (Bridges et al., 2010; Sato et al., 2008), which is modulated periodically in the helical structure. The data establish both the identity of the secondary structure and

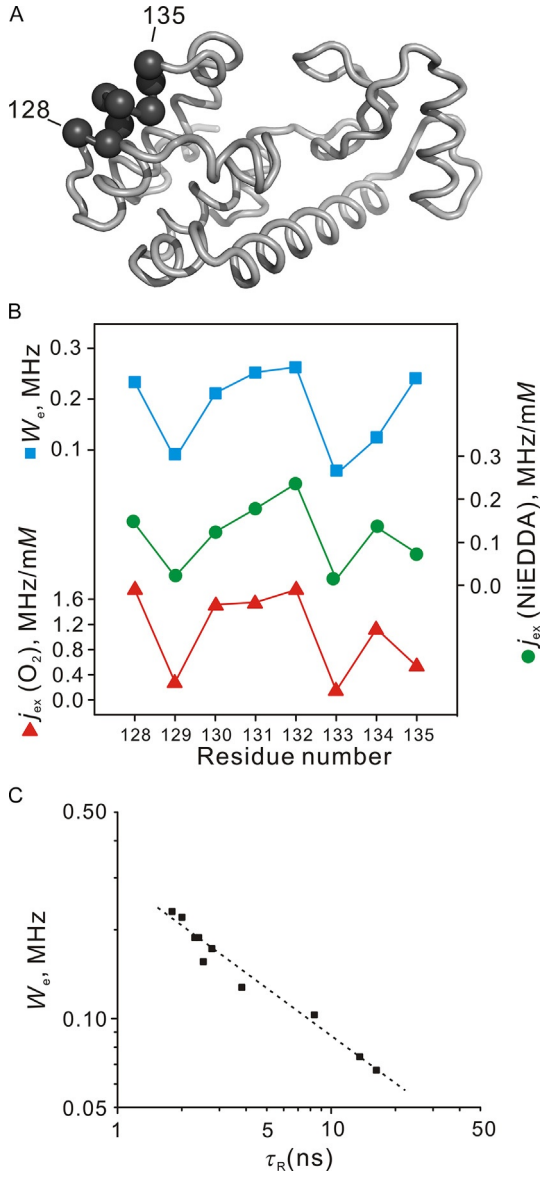

Figure 2 Determination of secondary structure with saturation recovery EPR. (A) Sites of sequential introduction of R1 along a helical segment in T4L; spheres mark the position of the C_α carbon atom of the labeled side chains. (B) The intrinsic spin–lattice relaxation rates measured in the absence of O_2 (W_e, blue (gray in the print version) squares) and rate constants obtained in the presence of O_2 (red (gray in the print version) triangles) or NiEDDA (green (gray in the print version) circles) are plotted as a function of residue number.

(Continued)

its orientation within the protein fold. Measurement of distances between residues in different secondary structural elements can provide information on the tertiary fold and that subject is considered next.

4.2 Measuring Interspin Distances with Relaxation Enhancement

Long-range (tens of Angstroms) distance measurement is a key tool in the elucidation of tertiary structure, structural changes, and structural heterogeneity in proteins, and SDSL-EPR spectroscopy is one of the most powerful techniques for this purpose. The most popular approach in this regard is pulsed dipolar spectroscopy (PDS), which includes double electron–electron resonance (DEER) and double-quantum coherence. Both spectroscopic techniques report the strength of the magnetic dipolar interaction between two spins using specifically tailored pulsed sequences (Borbat & Freed, 2014; Jeschke, 2012). The approximate distances measurable via PDS using R1 range from 12 to 70 Å. A unique feature of PDS is that the distance distributions may be determined in addition to most probable distances, but a disadvantage is that the method is typically carried out in frozen solution at cryogenic temperatures (50–80 K). We also note that recent studies utilizing the triarylmethyl (TAM) radical or spirocyclohexyl spin labels have reported progress in performing PDS near room temperature in proteins, although the practical upper limit of measurable distances using these radicals is relatively short (~35 Å) (Meyer et al., 2015; Yang et al., 2012).

An alternative to PDS for interspin distance measurements is the relaxation enhancement (RE) method. In RE, the enhancement of spin–lattice relaxation rate (W_e) for a spin label due to the presence of a second nearby spin is measured with SR. An endogenous or introduced paramagnetic metal is used as the second spin and the measured RE is proportional to r^{-6}, where r is the nitroxide-metal interspin distance. In contrast to PDS, RE provides only an average distance without resolving the distance distribution. However, RE can be measured with equal ease at both room and cryogenic temperatures, and PDS can be carried out on the same sample at cryogenic temperature. From the PDS distance distribution obtained,

Figure 2—Cont'd A clear periodicity is observed in all three cases, reflecting the helical nature of the T4L segment between residues 128–135. (C) The dependence of nitroxide W_e on the rotational correlation time (τ_R). W_e for R1 at various sites in T4L (differed from those shown in A) were obtained with a long-pulse SR experiment, and τ_R values were estimated from simulations of the CW spectra. *Replotted using data from Bridges et al. (2010).*

the expected RE can be computed and compared with experimental data. This capability can be used to test the effect of freezing on the protein structure and to aid in the interpretation of the RE data (Yang et al., 2014) (see example below). At room temperature, nitroxide/Cu^{2+} RE has measured interspin distances of up to 40 Å in proteins (Yang et al., 2014), although the use of TAM/Cu^{2+} pairs should permit measurement of distances up to ~50 Å (see below).

In the following, only RE distance measurements using a nitroxide spin label and a paramagnetic metal ion introduced site specifically are considered. The paramagnetic metal ion for RE-based distance measurements should have a T_{1e} within one or two orders of magnitude of ω^{-1}, where ω is the resonant frequency of the nitroxide. At X-band, $\omega \approx 10^{11}\ s^{-1}$ and Cu^{2+} with a T_{1e} of 1–5 ns is a suitable choice (Bertini et al., 2001; Jun, Becker, Yonkunas, Coalson, & Saxena, 2006). For a protein which does not contain an endogenous Cu^{2+}-binding site, a Cu^{2+}-binding motif compatible with the protein must be introduced site selectively. The affinity of the site must be much higher than that for nonspecific sites, which typically have K_d in the μM range. Recently, reported high-affinity Cu^{2+}-binding motifs (Fig. 3A) include a tripeptide sequence, GGH, which mimics the metal-binding site of Albumin (Yang et al., 2014); a double Histidine mutations in combination with an iminodiacetate ligand, dHis-IDA (Cunningham, Putterman, Desai, Horne & Saxena, 2015); and an EDTA-derivative Cu^{2+} chelate modified to react with a protein cysteine (Cunningham, Shannon, et al., 2015). The tripeptide GGH sequence provides a means for introducing Cu^{2+} in loop regions, while the dHis-IDA motif is suitable for helical or β-strand sequences (Cunningham, Putterman, et al., 2015); each has $K_d \ll 1\ \mu M$. In addition to high-binding affinity, internal flexibility of the engineered Cu^{2+} motif should be minimal because high flexibility would reduce the spatial resolution of the method and possibly introduce another potential T_{1e} relaxation pathway (via dynamic modulation of the interspin distance) (Yang et al., 2014). The tripeptide and the EDTA Cu^{2+} complexes were reported to have an internal flexibility comparable to that of the commonly used R1 side chain (Cunningham, Shannon, et al., 2015; Yang et al., 2014), while the dHis-IDA-Cu^{2+} complex is apparently very well-localized spatially (Cunningham, Putterman, et al., 2015).

The nitroxide can be introduced using cysteine substitution mutagenesis followed by reaction with a sulfhydryl-specific nitroxide reagent. The choice of nitroxide side chain is important: the longer the T_{1e} of the nitroxide, the longer the maximum distance that can be determined by

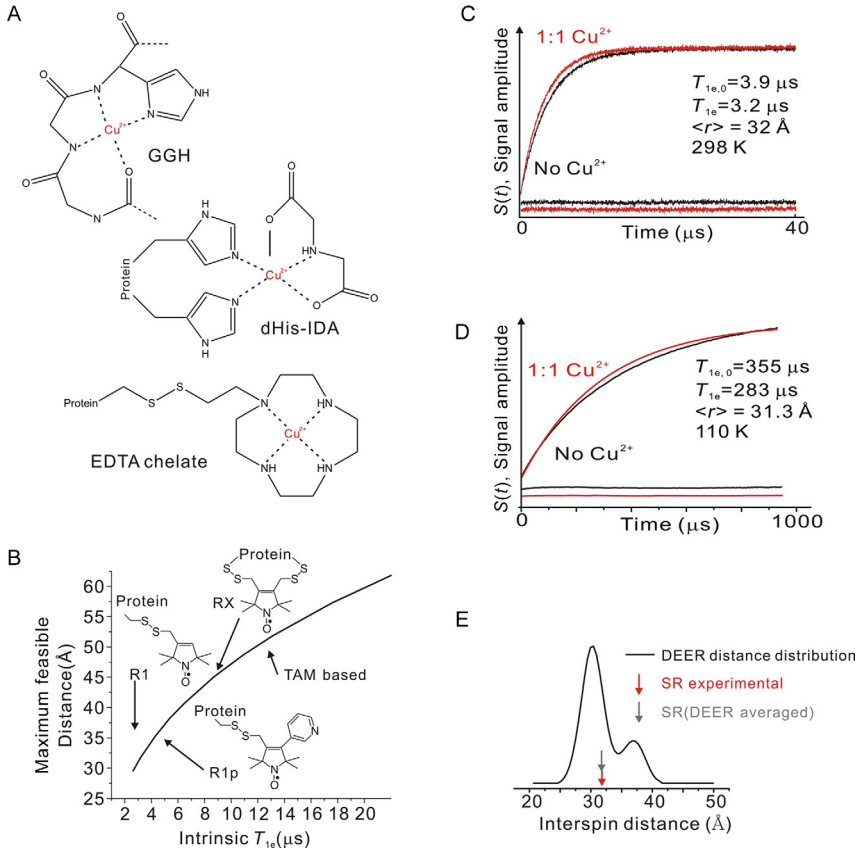

Figure 3 Determination of interspin distances in proteins with saturation recovery EPR. (A) Structures of ligands used to introduce Cu^{2+}-binding sites in proteins. (B) The maximum feasible Cu^{2+}/nitroxide distance that can be measured using the RE approach as a function of the intrinsic T_{1e} of the nitroxide. Structures of spin labels R1, R1p, RX are shown as insets, with arrows indicating their relaxation times and maximum distances feasible to measure. (C) and (D) Examples of RE of R1p by Cu^{2+} in the GGH loop-binding motif at 298 and 110 K, respectively; R1p is attached at site 131 in T4L, and GGH is inserted at site 23 (Yang et al., 2014). The relaxations in the presence (red (gray in the print version)) and absence (black) of Cu^{2+} were fit with single exponentials, and the residuals are shown. The mean distance measured at 298 K was computed according to the fast motion model while that at 110 K was obtained using the rigid limit model. Values of T_{1e} in the presence and absence of Cu^{2+} and the computed distances are shown in the inset. (E) The distance distribution of the Cu^{2+}-R1p distance in the same sample obtained from DEER at cryogenic temperature. The interspin distance calculated from room temperature RE experiments (red (light gray in the print version) arrow) is consistent with the "DEER average" distance corresponding to a sum of simulated exponentials weighted based on the experimental DEER distance distribution (gray arrow) (see Yang et al., 2014).

RE with Cu^{2+} (Fig. 3B; Yang et al., 2014). At room temperature, T_{1e} of an R1 side chain at surface sites is typically 1.5–2.5 μs depending on local structure and dynamics at the site, thus giving a maximal measurable interspin distance of ~25 Å (Jun et al., 2006). According to Fig. 2C, T_{1e} is inversely related to the correlation time of the nitroxide. Thus, nitroxide side chains with hindered internal motions are desired. These include R1p (Fawzi et al., 2011), V1 (Toledo Warshaviak, Khramtsov, Cascio, Altenbach, & Hubbell, 2013), and RX (Fleissner et al., 2011), which should allow for distance measurements up to 35 and 40 Å via RE at room temperature (Fig. 3B; Yang et al., 2014). In addition, with the long T_{1e} of the TAM radical (≈20 μs) (Owenius, Eaton & Eaton, 2005), it should be possible to measure distances up to 50 Å at room temperature. Spin-labeling reagents to introduce R1, R1p, V1, and RX at cysteine residues are now commercially available (Toronto Research Chemicals; Enzo life sciences), although the TAM-labeling reagent still requires custom synthesis (Yang et al., 2012). We also note that if a cysteine residue is used to introduce a Cu^{2+} chelate, an orthogonal chemistry is necessary to introduce the nitroxide side chain, for example, using an unnatural amino acid (Fleissner, Brustad, et al., 2009; Razzaghi et al., 2013). At the present time, nitroxides introduced in this fashion have high internal mobility and therefore short relaxation times, limiting the maximum distance measurable.

Once a nitroxide spin label and Cu^{2+} are introduced into a protein, interspin distance determinations require measurement of the nitroxide RE due to the metal ion, i.e., $RE = (T_{1e})^{-1} - (T_{1e}^0)^{-1}$, where T_{1e} and T_{1e}^0 are relaxation times in the presence and absence of Cu^{2+}, respectively. Interpretation of RE in terms of interspin distance depends on the rotational correlation time of the nitroxide–Cu^{2+} interspin vector, which is essentially the correlation time of the protein (τ_c) for the rigid nitroxide side chains and Cu^{2+} ligands considered above. Analytical expressions relating RE to interspin distance have been obtained for two models: in the fast motional limit the static magnetic dipolar interaction is completely averaged by rotational diffusion, while in the rigid limit, no such averaging occurs (Hirsh & Brudvig, 2007; Jun et al., 2006). In the case of Cu^{2+}/nitroxide interaction, the choice of model depends on both τ_c and the strength of the dipolar interaction (proportional to r^{-3}) according to (Yang et al., 2014):

$$5.3 \times 10^{11}\left[\frac{\tau_c}{r^3}\right] \begin{cases} \ll 1\,(\text{fast motional limit}) \\ > 1\,(\text{rigid limit}) \end{cases} \tag{5}$$

where r is the interspin distance in Angstroms. The fast motional limit is appropriate for small proteins (M.W. $<$ 20 kDa) and peptides in solution for the distance range of 25–40 Å (Jun et al., 2006; Yang et al., 2014). For shorter distances or somewhat larger proteins, the system will be in between the fast motional and rigid limits, but the correlation time can be "tuned" by increasing the viscosity of the medium or by attaching the protein to a solid support (López, Fleissner, Brooks, & Hubbell, 2014) in order to move the system to the rigid limit.

Analytical expressions that relate RE to interspin distance are (Yang et al., 2014).

At the fast motional limit,

$$\frac{1}{T_{1s}}-\frac{1}{T_{1s}^{0}}=\frac{2\pi^2 g_s^2 g_f^2 \beta_e^4}{5h^2 r^6}\left[\frac{T_{2f}}{1+(\omega_f-\omega_s)^2 T_{2f}^2}+\frac{3T_{1f}}{1+\omega_s^2 T_{1f}^2}+\frac{6T_{2f}}{1+(\omega_f+\omega_s)^2 T_{2f}^2}\right] \quad (6)$$

and at the rigid limit,

$$\frac{1}{T_{1s}}-\frac{1}{T_{1s}^{0}}=\frac{4\pi^2 g_s^2 g_f^2 \beta_e^4}{h^2 r^6}\left[\frac{T_{2f}}{1+(\omega_f-\omega_s)^2 T_{2f}^2}\left(1-3\cos^2\theta\right)^2 + \frac{3T_{1f}}{1+\omega_s^2 T_{1f}^2}\sin^2\theta\cos^2\theta+\frac{6T_{2f}}{1+(\omega_f+\omega_s)^2 T_{2f}^2}\sin^4\theta\right] \quad (7)$$

The parameters in Eqs. [6] and [7] are: μ_0, h, and β_e, the vacuum permeability, Planck constant, and the Bohr magneton, respectively; g_f and g_s, the g values for Cu^{2+} and the nitroxide (the fast and slowly relaxing species), respectively; ω_f and ω_s, the resonant frequencies for Cu^{2+} and the nitroxide, respectively; T_{1s} and T_{1s}^0, the spin–lattice relaxation times for the nitroxide in the presence and absence of Cu^{2+}, respectively; lastly, T_{1f} and T_{2f}, the spin–lattice and spin–spin relaxation times for Cu^{2+}. In the rigid limit, the calculation of the interspin distance requires integration over the angle θ, the angle between the interspin vector and the external magnetic field.

Examples of RE of R1p by Cu^{2+} chelated in the GGH loop in T4L are provided in Fig. 3C and D for 298 and 110 K, respectively, along with residuals for single-exponential fits to the data that give the indicated relaxation times. The distances computed from Eqs. [6] (at 298 K) and [7] (at 110 K) are in good agreement, suggesting little effect due to freezing on this sample. This is further supported by the Cu^{2+}/nitroxide DEER data obtained on the

same sample at 80 K, which showed that the weighted average distance computed from the DEER distribution (Sarver, Silva, & Saxena, 2013) is identical to that determined by RE (Fig. 3E).

4.3 Measuring Protein Conformational Exchange with T_1 Exchange Spectroscopy

It is now recognized that molecular flexibility is an inherent property of proteins in solution, and it can account for many aspects of function, including promiscuity of protein–protein interaction (James, Roversi, & Tawfik, 2003), enzyme catalysis (Eisenmesser et al., 2005), protein evolution (James et al., 2003), and allostery (Hilser, Wrabl, & Motlagh, 2012). The time scale of flexibility extends from ps–ns for backbone and side chain fluctuations to μs–ms for conformational exchanges (Henzler-Wildman & Kern, 2007). Remarkably, it appears that the *lifetimes* of individual substates involved in the fluctuating structures may be as important as the structural differences (Manglik et al., 2015).

Recent developments in SDSL have shown that the CW EPR spectra of R1 at select sites can measure the dynamics of fast (ps–ns) backbone fluctuations (Columbus & Hubbell, 2004; López, Oga, & Hubbell, 2012) and that the existence of two conformational substates in slow exchange (μs–ms) may be revealed by two-component EPR spectra as indicated in Fig. 4A (López, Fleissner, Guo, Kusnetzow, & Hubbell, 2009; López et al., 2012). However, exchange between two rotamers of the nitroxide can also give rise to resolved spectral components (Fig. 4B). To enable SDSL-EPR to detect true conformational exchange, it is thus essential to distinguish protein conformational variation from R1 rotameric exchange as the origin of observed two-component EPR spectra. Evidence to date indicates that long-pulse SR is effective for achieving this goal as well as for estimating conformational exchange rates.

Consider a spin label in equilibrium exchange between two environments in a protein, α and β, with the nitroxide being free of protein contacts in α but immobilized due to local interactions in β (Fig. 4A):

$$\alpha \underset{k_r}{\overset{k_f}{\rightleftarrows}} \beta \tag{8}$$

The exchange rate constant is defined as $k_{ex} = \frac{1}{2}(k_f + k_r)$, with k_f and k_r being the forward and reverse rate constants, respectively. If the exchange

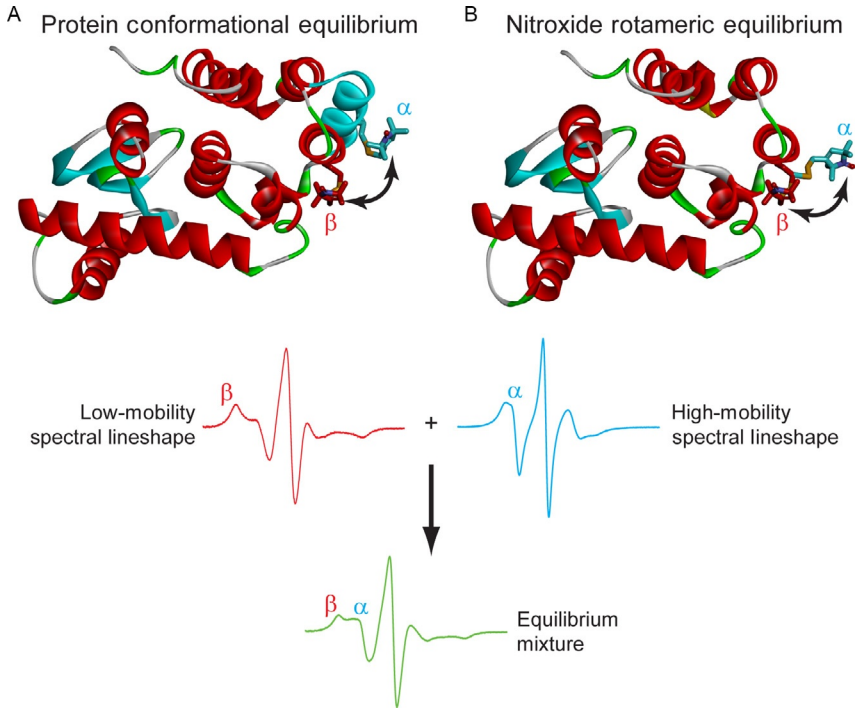

Figure 4 Structural origins of multicomponent CW EPR spectra. (A) Example of conformational exchange between two states related by the rotation of a helical segment. In one conformation (red (dark gray in the print version)), the nitroxide is immobilized due to interactions with the protein resulting in a broad spectral lineshape (β). In the other (rotated helix, cyan (light gray in the print version)), the interacting constraints are removed, resulting in a narrow resonance lineshape (α). In a slowly exchanging equilibrium mixture of these two states, the resulting spectrum is a sum of the two components in proportion to their population (green (gray in the print version) trace). (B) Two rotamers of a nitroxide side chain in a protein. In one rotamer, interaction with the protein results in an immobilized state (β), while in another, the constraints are removed, giving a mobile state (α). If the rotamer exchange is slow, the equilibrium mixture will consist of the sum of the two spectra, which is indistinguishable from the case of conformational exchange in (A).

lifetime, defined as $\tau_{ex} = k_{ex}^{-1}$, is $\geq$100 ns, the EPR spectrum of the mixture will be the algebraic sum of the spectra corresponding to α and β in proportion to the respective populations, and the lineshape will be unperturbed by the dynamic exchange event. On the other hand, the effective spin–lattice relaxation times will be strongly influenced by exchange events with lifetimes as long as $\approx$50 μs, providing an opportunity for SR to explore a time scale of motion nearly three orders of magnitude slower than that

corresponding to lineshape effects. The analysis of SR data in terms of exchange kinetics is considered in detail by Bridges et al. (2010); the main points that allow the distinction between conformational and rotameric exchange is summarized below.

Because the T_{1e} of the nitroxide depends on its total rotational correlation time (Fig. 2C), the α and β states will, in general, have different intrinsic spin–lattice relaxation rates: $W_{e\alpha} = (2T_{1e\alpha})^{-1}$ and $W_{e\beta} = (2T_{1e\beta})^{-1}$. If the first-order exchange rate constant between the states is such that,

$$k_{ex} \ll \left| W_{e\alpha} - W_{e\beta} \right| \tag{9}$$

the process is in the slow exchange limit, and the SR recovery is biexponential with each relaxation rate equal to the intrinsic relaxation rate of the respective individual state.

In the fast exchange limit,

$$k_{ex} \gg \left| W_{e\alpha} - W_{e\beta} \right| \tag{10}$$

the SR relaxation will be monoexponential with an effective relaxation rate W_{eff} that is simply the population-weighted average of the individual rates:

$$W_{eff} = \frac{1}{2T_{1eff}} = f_\alpha W_{e\alpha} + f_\beta W_{e\beta} \tag{11}$$

where f_α and f_β are the fractional populations of the states.

In intermediate exchange,

$$k_{ex} \approx \left| W_{e\alpha} - W_{e\beta} \right| \tag{12}$$

Two-component EPR spectra and biexponential SR relaxations are observed, but the relaxation times are complex functions of k_{ex}, f_α, f_β, $W_{e\alpha}$, and $W_{e\beta}$ (Bridges et al., 2010).

Intrinsic T_{1e} values for mobile (α) and immobile (β) states of R1 are typically ≈2 μs and ≈6 μs, respectively, and $\left| W_{e\alpha} - W_{e\beta} \right| \approx 170$ kHz, setting the time scale for T_{1e} exchange spectroscopy roughly in the range of 20 kHz–2 MHz, or exchange lifetimes in the range of 0.5–50 μs.

Remarkably, all documented cases to date of two-component EPR spectra that arise from distinct rotamers of R1 in a single protein conformation fall in the fast exchange limit at temperatures near ambient, i.e., $\tau_{ex} < 0.5$ μs (Bridges et al., 2010). If this proves to be general, the observation of a single-exponential relaxation for a two-component EPR spectrum identifies rotamer exchange as the origin of the two-component spectrum.

Thus, SR complements osmotic perturbation SDSL-EPR (López et al., 2009) and high pressure SDSL-EPR (Lerch, Horwitz, McCoy, & Hubbell, 2013; McCoy & Hubbell, 2011) as strategies to distinguish rotamer exchange from conformational exchange in SDSL-EPR studies of protein dynamics.

If a two-component EPR spectrum and a biexponential SR relaxation are observed, it is possible in some cases to distinguish slow from intermediate exchange. Simulation of the two-component EPR spectrum using the microscopic order–macroscopic disorder model (Budil, Lee, Saxena, & Freed, 1996; Freed, 1976) provides values for the nitroxide rotational correlation times from which expected values of $T_{1e\alpha}$ and $T_{1e\beta}$ for slow exchange can be obtained (see example in Fig. 2C). If the experimentally determined time constants from the biexponential relaxation are comparable to the T_{1e} values obtained from simulations, the system is likely in slow exchange. Intermediate exchange will result in relaxation times significantly shorter than those estimated from the nitroxide rotational correlation times (Bridges et al., 2010).

A further test to distinguish the slow and intermediate exchange regimes is provided by establishing a dependence of W_{eff} for each component on the concentration of an exchange reagent that differentially modulates the two rates based on differences in solvent accessibility. In slow exchange, the two states are effectively isolated and a plot of W_{eff} versus C_R is linear for each with slopes equal to j_{ex} (Fig. 5A; Eq. 4); in intermediate exchange the plot is curved (Fig. 5B). However, the curvature is slight and its resolution requires SR data with a high signal-to-noise ratio. In ideal cases, it is possible to estimate the numerical value of k_{ex} in the 20 kHz–2 MHz regime from the W_{eff} versus C_R data by globally fitting the data set to analytical expressions for W_{eff} in intermediate exchange. The procedure is not robust due to the large number of parameters involved (f_α, f_β, k_{ex}, $W_{e\alpha}$, $W_{e\beta}$, $j_{ex\alpha}$, and $j_{ex\beta}$). The limitations and strategies involved for application of the method are discussed in detail by Bridges et al. (2010).

5. SUMMARY AND FUTURE DIRECTIONS

At the present stage of development, SR EPR in combination with SDSL is a unique tool for resolving sequence-specific secondary structure through measurement of solvent accessibility, for mapping global protein structure via long-range distance measurements (10–40 Å) at physiological temperatures, and for identifying slow (μs–ms) conformational exchange in

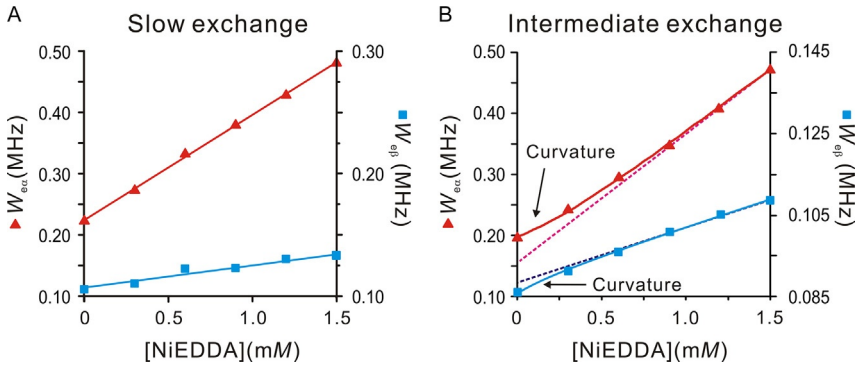

Figure 5 Distinguishing slow from intermediate exchange. (A) T4L 46R1 has a two-component EPR spectrum and a biexponential SR recovery due to slow exchange between two conformations of the protein. The relaxation rate for each component increases linearly with the concentration of an exchange reagent. (B) T4L 130R1 also has a two-component EPR spectrum and biexponential recovery. However, the relaxation rates are nonlinear functions of the exchange reagent concentration, a hallmark of intermediate exchange. The magenta (light gray in the print version) and dark blue (black in the print version) dashed lines are added to emphasize the nonlinearity of the fits. *Replotted with data from Bridges et al. (2010).*

proteins at equilibrium. In ideal cases, conformational exchange rates can also be estimated, but future developments in analytical methods will be required to improve the robustness of the measurements. For example, using SR relaxation amplitudes as well as rate data in a global analysis is one of the strategies under investigation. In addition, high pressure SR is an area for future development. Exchange events in general involve nonzero activation volumes, and pressure can be used to "titrate" exchange rates, providing an additional tool for exploring the time scale of exchange events. Finally, new spin labels with longer $T_{1e}s$ are desired to extend the range of distance measurements by RE. In this perspective, the TAM radical is a promising platform for future development.

REFERENCES

Altenbach, C., Froncisz, W., Hemker, R., McHaourab, H., & Hubbell, W. L. (2005). Accessibility of nitroxide side chains: Absolute Heisenberg exchange rates from power saturation EPR. *Biophysical Journal*, *89*(3), 2103–2112.

Berliner, L. J., Grunwald, J., Hankovszky, H. O., & Hideg, K. (1982). A novel reversible thiol-specific spin label: Papain active site labeling and inhibition. *Analytical Biochemistry*, *119*(2), 450–455.

Bertini, I., Luchinat, C., & Parigi, G. (Eds.), (2001). In *Current Methods in Inorganic Chemistry: Vol. 2. Solution NMR of paramagnetic molecules: Applications to metallobiomolecules and models* (pp. 1–372). New York: Elsevier Science.

Borbat, P., & Freed, J. (2014). Pulse dipolar ESR: Distance measurements. In J. Harmer & C. Timmel (Eds.), *Structure and bonding: Vol. 152. Structural information from spin-labels and intrinsic paramagnetic centers in the biosciences* (pp. 1–82). New York, USA: Springer. Heidelberg, Germany.

Bridges, M., Hideg, K., & Hubbell, W. (2010). Resolving conformational and rotameric exchange in spin-labeled proteins using saturation recovery EPR. *Applied Magnetic Resonance*, *37*(1–4), 363–390.

Budil, D. E., Lee, S., Saxena, S., & Freed, J. H. (1996). Nonlinear-least-squares analysis of slow-motion EPR spectra in one and two dimensions using a modified Levenberg-Marquardt algorithm. *Journal of Magnetic Resonance, Series A*, *120*(2), 155–189.

Columbus, L., & Hubbell, W. L. (2004). Mapping backbone dynamics in solution with site-directed spin labeling: GCN4-58 bZip free and bound to DNA. *Biochemistry*, *43*(23), 7273–7287.

Columbus, L., Kálai, T., Jekö, J., Hideg, K., & Hubbell, W. L. (2001). Molecular motion of spin labeled side chains in α-helices: Analysis by variation of side chain structure. *Biochemistry*, *40*(13), 3828–3846.

Cunningham, T. F., Putterman, M. R., Desai, A., Horne, W. S., & Saxena, S. (2015a). The double histidine Cu^{2+}-binding motif: A highly rigid, site-specific spin probe for electron spin resonance distance measurements. *Angewandte Chemie*, *54*(21), 6330–6334.

Cunningham, T. F., Shannon, M. D., Putterman, M. R., Arachchige, R. J., Sengupta, I., Gao, M., et al. (2015b). Cysteine-specific Cu2 + chelating tags used as paramagnetic probes in double electron electron resonance. *The Journal of Physical Chemistry. B*, *119*(7), 2839–2843.

Eaton, G. R., & Eaton, S. S. (2002). Determination of distances based on T_1 and T_m effects. In L. Berliner, G. Eaton, & S. Eaton (Eds.), *Distance measurements in biological systems by EPR: Vol. 19* (pp. 348–381). New York: Kluwer Academic/Plenum Publisher.

Eaton, S. S., & Eaton, G. R. (2005). Saturation recovery EPR. In S. S. Eaton, L. J. Berliner, & G. R. Eaton (Eds.), *Biological magnetic resonance Vol. 24. Biomedical EPR part B: Methodology, instrumentation, and dynamics* (pp. 3–18). New York City: Springer.

Eisenmesser, E. Z., Millet, O., Labeikovsky, W., Korzhnev, D. M., Wolf-Watz, M., Bosco, D. A., et al. (2005). Intrinsic dynamics of an enzyme underlies catalysis. *Nature*, *438*(7064), 117–121.

Fawzi, N., Fleissner, M., Anthis, N., Kálai, T., Hideg, K., Hubbell, W., et al. (2011). A rigid disulfide-linked nitroxide side chain simplifies the quantitative analysis of PRE data. *Journal of Biomolecular NMR*, *51*(1–2), 105–114.

Fleissner, M. R., Bridges, M. D., Brooks, E. K., Cascio, D., Kálai, T., Hideg, K., et al. (2011). Structure and dynamics of a conformationally constrained nitroxide side chain and applications in EPR spectroscopy. *Proceedings of the National Academy of Sciences of the United States of America*, *108*(39), 16241–16246.

Fleissner, M. R., Brustad, E. M., Kálai, T., Altenbach, C., Cascio, D., Peters, F. B., et al. (2009a). Site-directed spin labeling of a genetically encoded unnatural amino acid. *Proceedings of the National Academy of Sciences of the United States of America*, *106*(51), 21637–21642.

Fleissner, M. R., Cascio, D., & Hubbell, W. L. (2009b). Structural origin of weakly ordered nitroxide motion in spin-labeled proteins. *Protein Science*, *18*(5), 893–908.

Freed, J. H. (1974). Theory of saturation and double resonance in electron spin resonance spectra. VI. Saturation recovery. *The Journal of Physical Chemistry*, *78*(12), 1155–1167.

Freed, J. H. (1976). Theory of slow tumbling ESR spectra for nitroxides. In L. J. Berliner (Ed.), *Spin labeling theory and applications* (pp. 53–132). New York, NY: Academic Press.

Froncisz, W., Camenisch, T. G., Ratke, J. J., Anderson, J. R., Subczynski, W. K., Strangeway, R. A., et al. (2008). Saturation recovery EPR and ELDOR at W-band for spin labels. *Journal of Magnetic Resonance*, *193*(2), 297–304.

Guo, Z., Cascio, D., Hideg, K., Kálái, T., & Hubbell, W. L. (2007). Structural determinants of nitroxide motion in spin-labeled proteins: Tertiary contact and solvent-inaccessible sites in helix G of T4 lysozyme. *Protein Science*, *16*(6), 1069–1086.

Haas, D. A., Mailer, C., Sugano, T., & Robinson, B. A. (1992). New developments in pulsed electron paramagnetic resonance: Direct measurement of rotational correlation times from decay curves. *Bulletin of Magnetic Resonance*, *14*, 35–41.

Haas, D. A., Sugano, T., Mailer, C., & Robinson, B. H. (1993). Motion in nitroxide spin labels: Direct measurement of rotational correlation times by pulsed electron double resonance. *The Journal of Physical Chemistry*, *97*(12), 2914–2921.

Henzler-Wildman, K., & Kern, D. (2007). Dynamic personalities of proteins. *Nature*, *450*(7172), 964–972.

Hilser, V. J., Wrabl, J. O., & Motlagh, H. N. (2012). Structural and energetic basis of allostery. *Annual Review of Biophysics*, *41*(1), 585–609.

Hirsh, D. J., & Brudvig, G. W. (2007). Measuring distances in proteins by saturation-recovery EPR. *Nature Protocols*, *2*(7), 1770–1781.

Hubbell, W. L., & Altenbach, C. (1994). Investigation of structure and dynamics in membrane proteins using site-directed spin labeling. *Current Opinion in Structural Biology*, *4*(4), 566–573.

Hubbell, W. L., Froncisz, W., & Hyde, J. S. (1987). Continuous and stopped flow EPR spectrometer based on a loop gap resonator. *Review of Scientific Instruments*, *58*(10), 1879–1886.

Hubbell, W. L., Gross, A., Langen, R., & Lietzow, M. A. (1998). Recent advances in site-directed spin labeling of proteins. *Current Opinion in Structural Biology*, *8*(5), 649–656.

Huisjen, M., & Hyde, J. S. (1974). A pulsed EPR spectrometer. *Review of Scientific Instruments*, *45*(5), 669–675.

Hyde, J. S. (1979). Saturation recovery methodology. In L. Kevan & R. N. Schwartz (Eds.), *Time domain electron spin resonance* (pp. 1–30). New York City, NY: John Iley & Sons, INC.

Hyde, J. S., Chien, J. C. W., & Freed, J. H. (1968). Electron–electron double resonance of free radicals in solution. *The Journal of Chemical Physics*, *48*(9), 4211–4226.

Hyde, J. S., Yin, J.-J., Froncisz, W., & Feix, J. B. (1985). Electron–electron double resonance (ELDOR) with a loop-gap resonator. *Journal of Magnetic Resonance*, *63*(1), 142–150.

Isas, J. M., Langen, R., Haigler, H. T., & Hubbell, W. L. (2002). Structure and dynamics of a helical hairpin and loop region in annexin 12: A site-directed spin labeling study. *Biochemistry*, *41*(5), 1464–1473.

James, L. C., Roversi, P., & Tawfik, D. S. (2003). Antibody multispecificity mediated by conformational diversity. *Science*, *299*(5611), 1362–1367.

Jeschke, G. (2012). DEER distance measurements on proteins. *Annual Review of Physical Chemistry*, *63*(1), 419–446.

Jun, S., Becker, J. S., Yonkunas, M., Coalson, R., & Saxena, S. (2006). Unfolding of alanine-based peptides using electron spin resonance distance measurements. *Biochemistry*, *45*(38), 11666–11673.

Kawasaki, K., Yin, J.-J., Subczynski, W. K., Hyde, J. S., & Kusumi, A. (2001). Pulse EPR detection of lipid exchange between protein-rich raft and bulk domains in the membrane: Methodology development and its application to studies of influenza viral membrane. *Biophysical Journal*, *80*(2), 738–748.

Kusumi, A., Subczynski, W. K., & Hyde, J. S. (1982). Oxygen transport parameter in membranes as deduced by saturation recovery measurements of spin–lattice relaxation times of spin labels. *Proceedings of the National Academy of Sciences of the United States of America*, *79*(6), 1854–1858.

Lerch, M. T., Horwitz, J., McCoy, J., & Hubbell, W. L. (2013). Circular dichroism and site-directed spin labeling reveal structural and dynamical features of high-pressure states of myoglobin. *Proceedings of the National Academy of Sciences of the United States of America*, *110*(49), E4714–E4722.

Lin, Y., Nielsen, R., Murray, D., Hubbell, W. L., Mailer, C., Robinson, B. H., et al. (1998). Docking phospholipase A2 on membranes using electrostatic potential-modulated spin relaxation magnetic resonance. *Science*, *279*(5358), 1925–1929.

López, C. J., Fleissner, M. R., Brooks, E. K., & Hubbell, W. L. (2014). Stationary-phase EPR for exploring protein structure, conformation, and dynamics in spin-labeled proteins. *Biochemistry*, *53*(45), 7067–7075.

López, C. J., Fleissner, M. R., Guo, Z., Kusnetzow, A. K., & Hubbell, W. L. (2009). Osmolyte perturbation reveals conformational equilibria in spin-labeled proteins. *Protein Science*, *18*(8), 1637–1652.

López, C. J., Oga, S., & Hubbell, W. L. (2012). Mapping molecular flexibility of proteins with site-directed spin labeling: A case study of myoglobin. *Biochemistry*, *51*(33), 6568–6583.

Mailer, C., Nielsen, R. D., & Robinson, B. H. (2005). Explanation of spin–lattice relaxation rates of spin labels obtained with multifrequency saturation recovery EPR. *The Journal of Physical Chemistry. A*, *109*(18), 4049–4061.

Manglik, A., Kim, T. H., Masureel, M., Altenbach, C., Yang, Z., Hilger, D., et al. (2015). Structural insights into the dynamic process of β2-adrenergic receptor signaling. *Cell*, *161*(5), 1101–1111.

McCoy, J., & Hubbell, W. L. (2011). High-pressure EPR reveals conformational equilibria and volumetric properties of spin-labeled proteins. *Proceedings of the National Academy of Sciences of the United States of America*, *108*(4), 1331–1336.

Meyer, V., Swanson, M. A., Clouston, L. J., Boratyński, P. J., Stein, R. A., McHaourab, H. S., et al. (2015). Room-temperature distance measurements of immobilized spin-labeled protein by DEER/PELDOR. *Biophysical Journal*, *108*(5), 1213–1219.

Oh, K. J., Zhan, H., Cui, C., Hideg, K., Collier, R. J., & Hubbell, W. L. (1996). Organization of diphtheria toxin T domain in bilayers: A site-directed spin labeling study. *Science*, *273*(5276), 810–812.

Owenius, R., Eaton, G. R., & Eaton, S. S. (2005). Frequency (250 MHz to 9.2 GHz) and viscosity dependence of electron spin relaxation of triarylmethyl radicals at room temperature. *Journal of Magnetic Resonance*, *172*(1), 168–175.

Owenius, R., Terry, G. E., Williams, M. J., Eaton, S. S., & Eaton, G. R. (2004). Frequency dependence of electron spin relaxation of nitroxyl radicals in fluid solution. *The Journal of Physical Chemistry. B*, *108*(27), 9475–9481.

Percival, P. W., & Hyde, J. S. (1975). Pulsed EPR spectrometer, II. *Review of Scientific Instruments*, *46*(11), 1522–1529.

Popp, C. A., & Hyde, J. S. (1982). Electron–electron double resonance and saturation-recovery studies of nitroxide electron and nuclear spin–lattice relaxation times and Heisenberg exchange rates: Lateral diffusion in dimyristoyl phosphatidylcholine. *Proceedings of the National Academy of Sciences of the United States of America*, *79*(8), 2559–2563.

Pyka, J., Ilnicki, J., Altenbach, C., Hubbell, W. L., & Froncisz, W. (2005). Accessibility and dynamics of nitroxide side chains in T4 lysozyme measured by saturation recovery EPR. *Biophysical Journal*, *89*(3), 2059–2068.

Razzaghi, S., Brooks, E. K., Bordignon, E., Hubbell, W. L., Yulikov, M., & Jeschke, G. (2013). EPR relaxation-enhancement-based distance measurements on orthogonally spin-labeled T4-lysozyme. *ChemBioChem*, *14*(14), 1883–1890.

Robinson, B. H., Haas, D. A., & Mailer, C. (1994). Molecular dynamics in liquids: Spin–lattice relaxation of nitroxide spin labels. *Science*, *263*(5146), 490–493.

Sarver, J., Silva, K. I., & Saxena, S. (2013). Measuring Cu2+-nitroxide distances using double electron–electron resonance and saturation recovery. *Applied Magnetic Resonance*, *44*(5), 583–594.

Sato, H., Bottle, S. E., Blinco, J. P., Micallef, A. S., Eaton, G. R., & Eaton, S. S. (2008). Electron spin–lattice relaxation of nitroxyl radicals in temperature ranges that span glassy solutions to low-viscosity liquids. *Journal of Magnetic Resonance*, *191*(1), 66–77.

Shin, Y. K., & Hubbell, W. L. (1992). Determination of electrostatic potentials at biological interfaces using electron–electron double resonance. *Biophysical Journal*, *61*(6), 1443–1453.

Subczynski, W. K., Hyde, J. S., & Kusumi, A. (1989). Oxygen permeability of phosphatidylcholine—Cholesterol membranes. *Proceedings of the National Academy of Sciences of the United States of America*, *86*(12), 4474–4478.

Subczynski, W. K., Hyde, J. S., & Kusumi, A. (1991). Effect of alkyl chain unsaturation and cholesterol intercalation on oxygen transport in membranes: A pulse ESR spin labeling study. *Biochemistry*, *30*(35), 8578–8590.

Sugano, T., Mailer, C., & Robinson, B. H. (1987). Direct detection of very slow two-jump processes by saturation recovery electron paramagnetic resonance spectroscopy. *The Journal of Chemical Physics*, *87*(5), 2478–2488.

Teng, C.-L., Hong, H., Kiihne, S., & Bryant, R. G. (2001). Molecular oxygen spin–lattice relaxation in solutions measured by proton magnetic relaxation dispersion. *Journal of Magnetic Resonance*, *148*(1), 31–34.

Toledo Warshaviak, D., Khramtsov, V. V., Cascio, D., Altenbach, C., & Hubbell, W. L. (2013). Structure and dynamics of an imidazoline nitroxide side chain with strongly hindered internal motion in proteins. *Journal of Magnetic Resonance*, *232*, 53–61.

Yang, Z., Jiménez-Osés, G., López, C. J., Bridges, M. D., Houk, K. N., & Hubbell, W. L. (2014). Long-range distance measurements in proteins at physiological temperatures using saturation recovery EPR spectroscopy. *Journal of the American Chemical Society*, *136*(43), 15356–15365.

Yang, Z., Liu, Y., Borbat, P., Zweier, J. L., Freed, J. H., & Hubbell, W. L. (2012). Pulsed ESR dipolar spectroscopy for distance measurements in immobilized spin labeled proteins in liquid solution. *Journal of the American Chemical Society*, *134*(24), 9950–9952.

Yin, J.-J., & Hyde, J. S. (1987). Spin-label saturation-recovery electron spin resonance measurements of oxygen transport in membranes. *Zeitschrift für Physikalische Chemie*, *153*, 57–65.

Yin, J.-J., & Hyde, J. S. (1989). Use of high observing power in electron spin resonance saturation-recovery experiments in spin-labeled membranes. *The Journal of Chemical Physics*, *91*(10), 6029–6035.

Yin, J. J., Pasenkiewicz-Gierula, M., & Hyde, J. S. (1987). Lateral diffusion of lipids in membranes by pulse saturation recovery electron spin resonance. *Proceedings of the National Academy of Sciences of the United States of America*, *84*(4), 964–968.